

On Similarity of Seismo Radial Grain Velocity and Capillary Pressure Fractal Dimension for Characterizing Shajara Reservoirs of the Permoo-Carboniferous Shajara Formation, Saudi Arabia

Khalid Elyas Mohamed Elameen Alkhidir

Ph.D. Department of Petroleum and Natural Gas Engineering,
College of Engineering, King Saud University, Saudi Arabia

*Corresponding author

Prof. Khalid Elyas Mohamed Elameen Alkhidir, Ph.D. Department of Petroleum and Natural Gas Engineering, College of Engineering, King Saud University, Saudi Arabia

Submitted: 30 Jan 2020; Accepted: 06 Feb 2020; Published: 14 Feb 2020

The quality and assessment of a reservoir can be documented in details by the application of seismo radial grain velocity. This research aims to calculate fractal dimension from the relationship among seismo radial grain velocity, maximum seismo radial grain velocity and wetting phase saturation and to approve it by the fractal dimension derived from the relationship among capillary pressure and wetting phase saturation. Two equations for calculating the fractal dimensions have been employed. The first one describes the functional relationship between wetting phase saturation, seismo radial grain velocity, maximum seismo radial grain velocity and fractal dimension. The second equation implies to the wetting phase saturation as a function of capillary pressure and the fractal dimension. Two procedures for obtaining the fractal dimension have been utilized. The first procedure was done by plotting the logarithm of the ratio between seismo radial grain velocity and maximum seismo radial grain velocity versus logarithm wetting phase saturation. The slope of the first procedure = $3 - D_f$ (fractal dimension). The second procedure for obtaining the fractal dimension was determined by plotting the logarithm of capillary pressure versus the logarithm of wetting phase saturation. The slope of the second procedure = $D_f - 3$. On the basis of the obtained results of the fabricated stratigraphic column and the attained values of the fractal dimension, the sandstones of the Shajara reservoirs of the Shajara Formation were divided here into three units.

Keywords: Shajara Reservoirs; Shajara Formation; Seismo radial grain velocity fractal dimension; Capillary pressure fractal dimension, Permeability

Introduction

Seismo electric effects related to electro kinetic potential, dielectric permittivity, pressure gradient, fluid viscosity, and electric conductivity was first reported by [1]. Capillary pressure follows the scaling law at low wetting phase saturation was reported by [2]. Seismo electric phenomenon by considering electro kinetic coupling coefficient as a function of effective charge density, permeability, fluid viscosity and electric conductivity was reported by [3]. The magnitude of seismo electric current depends on porosity, pore size, zeta potential of the pore surfaces, and elastic properties of the matrix was investigated by [4]. The tangent of the ratio of converted electric field to pressure is approximately in inverse proportion to permeability was studied by [5]. Permeability inversion from seismo electric log at low frequency was studied by [6]. They reported that, the tangent of the ratio among electric excitation intensity and pressure field is a function of porosity, fluid viscosity, frequency, tortuosity and fluid density and Dracy permeability. A decrease of seismo electric frequencies with increasing water content was reported by [7]. An increase of

seismo electric transfer function with increasing water saturation was studied by [8]. An increase of dynamic seismo electric transfer function with decreasing fluid conductivity was described by [9]. The amplitude of seismo electric signal increases with increasing permeability which means that the seismo electric effects are directly related to the permeability and can be used to study the permeability of the reservoir was illustrated by [10]. Seismo electric coupling is frequency dependent and decreases exponentially when frequency increases was demonstrated by [11]. An increase of permeability with increasing seismo magnetic moment and seismo diffusion coefficient fractal dimension was reported by [12, 13]. An increase of, molar enthalpy, work fractal, electro kinetic, bubble pressure and pressure head fractal dimensions with permeability increasing and grain size was described by [14,15,16,17].

Material and Method

Sandstone samples were collected from the surface type section of the Permoo-Carboniferous Shajara Formation, latitude $26^{\circ} 52' 17.4''$, longitude $43^{\circ} 36' 18''$. (Figure1). Porosity was measured on collected samples using mercury intrusion Porosimetry and permeability was derived from capillary pressure data. The purpose of this paper is to obtain seismo radial grain velocity fractal dimension and to confirm

it by capillary pressure fractal dimension. The fractal dimension of the first procedure is determined from the positive slope of the plot of logarithm of the ratio of seismo radial grain velocity to maximum seismo radial grain velocity $\log(SRGV_{1/4}/SRGV_{1/4max})$ versus \log wetting phase saturation ($\log Sw$). Whereas the fractal dimension of the second procedure is determined from the negative slope of the plot of logarithm of \log capillary pressure ($\log Pc$) versus logarithm of wetting phase saturation ($\log Sw$).

The Seismo radial grain velocity can be scaled as

AGE	Fm.	Mbr.	unit	LITHOLOGY	DESCRIPTION
Late Permian	Khuff Formation	Hagyl Member			Limestone : Cream, dense, burrowed, thickness 6.5'
					Sub-Khuff unconformity.
Late Carboniferous - Permian	Shajara Formation	Upper Shajara Member	Upper Shajara mudstone		Mudstone : Yellow, thickness 17.7'
			Upper Shajara Reservoir	SJ13▲	Sandstone : Light brown, cross-bedded, coarse-grained, poorly sorted, porous, friable, thickness 6.5'
				SJ12▲	Sandstone : Yellow, medium-grained, very coarse-grained, poorly, moderately sorted, porous, friable, thickness 13.1'
			Upper Shajara Reservoir	SJ11▲	Mudstone : Yellow-green, thickness 11.8'
					Mudstone : Yellow, thickness 1.3'
			Middle Shajara Member	Middle Shajara Reservoir	SJ10▲
		SJ9▲			Sandstone : Light brown, medium-grained, moderately sorted, porous, friable, thickness 3.6'
		SJ8▲			Sandstone : Yellow, medium-grained, moderately well sorted, porous, friable, thickness 0.9'
		SJ7▲			Sandstone : Red, coarse-grained, medium-grained, moderately well sorted, porous, friable, thickness 13.4'
		SJ6▲			Sandstone : White with yellow spots, fine-grained, hard, thickness 2.6'
		SJ5▲			Sandstone : Limonite, thickness 1.3'
		Lower Shajara Member	Lower Shajara Reservoir	SJ4▲	Sandstone : White, coarse-grained, very poorly sorted, thickness 4.5'
				SJ3▲	Sandstone : White-pink, poorly sorted, thickness 1.6'
				SJ2▲	Sandstone : Yellow, medium-grained, well sorted, porous, friable, thickness 3.9'
				SJ1▲	Sandstone : Red, medium-grained, moderately well sorted, porous, friable, thickness 11.8'
					Sub-Unayzah unconformity.
					Sandstone : White, fine-grained.

Figure 1: Surface type section of the Shajara Reservoirs of the Permo-Carboniferous Shajara Formation at latitude 26° 52' 17.4" longitude 43° 36' 18"

$$Sw = \left[\frac{SRGV_{1/4}^2}{SRGV_{max}^2} \right]^{[3-Df]} \quad (1)$$

Where Sw the water saturation, $SRGV$ the seismo radial grain velocity in meter / second, $SRGV_{max}$ the maximum seismo radial grain velocity in meter / second, and Df the fractal dimension.

Equation 1 can be proofed from

$$H = \left[\frac{\phi * \epsilon * Kf * \zeta * \rho f * SSWV * SRGV}{\alpha_{\infty} * \eta} \right] \quad (2)$$

Where H the magnetic field in ampere / meter, ϕ the porosity, ϵ the fluid permittivity in Faraday / meter, Kf the fluid dielectric constant, ζ the zeta potential in volt, ρf the fluid density in kilogram / cubic meter, $SSWV$ the seismic shear wave velocity in meter / second, $SRGV$ the seismo radial grain velocity in meter / second, α the tortuosity, η the fluid viscosity in pascal * second

The viscosity η can be scaled as

$$\eta = P * t \quad (3)$$

Where η the fluid viscosity in pascal * second, P the pressure in pascal, and t the time in second

Insert equation 3 into equation 2

$$H = \left[\frac{\phi * \epsilon * Kf * \zeta * \rho f * SSWV * SRGV}{\alpha_{\infty} * P * t} \right] \quad (4)$$

The time t can be scaled as

$$t = \left[\frac{V}{Q} \right] \quad (5)$$

Where t the time in second, V the volume in cubic meter, Q the flow rate in cubic meter / second

Insert equation 5 into equation 4

$$H = \left[\frac{\phi * \epsilon * Kf * \zeta * \rho f * SSWV * SRGV * Q}{\alpha_{\infty} * P * V} \right] \quad (6)$$

The volume V can be scaled as

$$V = A * h \quad (7)$$

Where V the volume in cubic meter, A the area in square meter, h the height in meter

Insert equation 7 into equation 6

$$H = \left[\frac{\phi * \epsilon * Kf * \zeta * \rho f * SSWV * SRGV * Q}{\alpha_{\infty} * P * A * h} \right] \quad (8)$$

The area A can be scaled as

$$A = \Pi * r^2 \quad (9)$$

Where A the area in square meter, Π constant, r the pore radius in meter

Insert equation 9 into equation 8

$$H = \left[\frac{\phi * \epsilon * Kf * \zeta * \rho f * SSWV * SRGV * Q}{\alpha_{\infty} * P * \Pi * r^2 * h} \right] \quad (10)$$

Equation 10 after rearrange will become

$$H * r^2 = \left[\frac{\phi * \epsilon * Kf * \zeta * \rho f * SSWV * SRGV * Q}{\alpha_{\infty} * P * \Pi * h} \right] \quad (11)$$

The maximum pore radius can be scaled as

$$H * r_{\max}^2 = \left[\frac{\phi * \epsilon * Kf * \zeta * \rho f * SSWV * SRGV_{\max} * Q}{\alpha_{\infty} * P * \Pi * h} \right] \quad (12)$$

Divide equation 11 by equation 12

$$\left[\frac{H * r^2}{H * r_{\max}^2} \right] = \left[\frac{\left[\frac{\phi * \epsilon * Kf * \zeta * \rho f * SSWV * SRGV * Q}{\alpha_{\infty} * P * \Pi * h} \right]}{\left[\frac{\phi * \epsilon * Kf * \zeta * \rho f * SSWV * SRGV_{\max} * Q}{\alpha_{\infty} * P * \Pi * h} \right]} \right] \quad (13)$$

Equation 13 after simplification will become

$$\left[\frac{r^2}{r_{\max}^2} \right] = \left[\frac{SRGV}{SRGV_{\max}} \right] \quad (14)$$

Take the square root of equation 14

$$\sqrt{\left[\frac{r^2}{r_{\max}^2} \right]} = \sqrt{\left[\frac{SRGV}{SRGV_{\max}} \right]} \quad (15)$$

Equation 15 after simplification will become

$$\left[\frac{r}{r_{\max}} \right] = \left[\frac{SRGV^{\frac{1}{2}}}{SRGV_{\max}^{\frac{1}{2}}} \right] \quad (16)$$

Take the logarithm of equation 16

$$\log \left[\frac{r}{r_{\max}} \right] = \log \left[\frac{SRGV^{\frac{1}{2}}}{SRGV_{\max}^{\frac{1}{2}}} \right] \quad (17)$$

$$\text{But; } \log \left[\frac{r}{r_{\max}} \right] = \left[\frac{\log Sw}{3 - Df} \right] \quad (18)$$

Insert equation 18 into equation 17

$$\left[\frac{\log Sw}{3 - Df} \right] = \log \left[\frac{SRGV^{\frac{1}{2}}}{SRGV_{\max}^{\frac{1}{2}}} \right] \quad (19)$$

Equation 19 after log removal will become

$$Sw = \left[\frac{SRGV^{\frac{1}{2}}}{SRGV_{\max}^{\frac{1}{2}}} \right]^{[3 - Df]} \quad (20)$$

Equation 20 the proof of equation 1 which relates the water saturation, seismo radial grain velocity, maximum seismo radial grain velocity, and the fractal dimension.

The capillary pressure can be scaled as

$$\text{LogSw} = [Df - 3] * \log pc + \text{constant} \quad (21)$$

Where Sw the water saturation, Pc the capillary pressure and Df the fractal dimension.

Results and Discussion

Based on field observation the Shajara Reservoirs of the Permo-Carboniferous Shajara Formation were divided here into three units as described in Figure 1. These units from bottom to top are: Lower Shajara Reservoir, Middle Shajara reservoir, and Upper Shajara Reservoir. Their attained results of the seismo radial grain velocity fractal dimension and capillary pressure fractal dimension are shown in Table 1. Based on the achieved results it was found that the seismo radial grain velocity fractal dimension is equal to the capillary pressure fractal dimension. The maximum value of the fractal dimension was found to be 2.7872 allocated to sample SJ13 from the Upper Shajara Reservoir as verified in Table 1. Whereas the minimum value of the fractal dimension 2.4379 was reported from sample SJ3 from the Lower Shajara reservoir as shown in Table 1. The Seismo radial grain velocity fractal dimension and capillary pressure fractal dimension were detected to increase with increasing permeability as proofed in Table 1 owing to the possibility of having interconnected channels.

Table 1: Petrophysical model showing the three Shajara Reservoir Units with their corresponding values of seismo radial grain velocity fractal dimension and capillary pressure fractal dimension

Formation	Reservoir	Sample	Porosity %	k (md)	Positive slope of the first procedure Slope=3-Df	Negative slope of the second procedure Slope=Df-3	Seismo radial grain velocity fractal dimension	Capillary pressure fractal dimension
Shajara Formation	Upper Shajara Reservoir	SJ13	25	973	0.2128	-0.2128	2.7872	2.7872
		SJ12	28	1440	0.2141	-0.2141	2.7859	2.7859
		SJ11	36	1197	0.2414	-0.2414	2.7586	2.7586
	Middle Shajara Reservoir	SJ9	31	1394	0.2214	-0.2214	2.7786	2.7786
		SJ8	32	1344	0.2248	-0.2248	2.7752	2.7752
		SJ7	35	1472	0.2317	-0.2317	2.7683	2.7683
	Lower Shajara Reservoir	SJ4	30	176	0.3157	-0.3157	2.6843	2.6843
		SJ3	34	56	0.5621	-0.5621	2.4379	2.4379
		SJ2	35	1955	0.2252	-0.2252	2.7748	2.7748
		SJ1	29	1680	0.2141	-0.2141	2.7859	2.7859

The Lower Shajara reservoir was symbolized by six sandstone samples (Figure 1), four of which label as SJ1, SJ2, SJ3 and SJ4 were carefully chosen for capillary pressure measurement as proven in Table 1. Their positive slopes of the first procedure log of the Seismo radial grain velocity to maximum Seismo radial grain velocity versus log wetting phase saturation (Sw) and negative slopes of the second procedure log capillary pressure (Pc) versus log wetting phase saturation (Sw) are clarified in Figure 2, Figure 3, Figure 4, Figure 5 and Table 1. Their Seismo radial grain velocity fractal dimension and capillary pressure fractal dimension values are revealed in Table 1. As we proceed from sample SJ2 to SJ3 a pronounced reduction in permeability due to compaction was described from 1955 md to 56 md which reflects decrease in Seismo radial grain velocity fractal dimension from 2.7748 to 2.4379 as quantified in table 1. Again, an increase in grain size and permeability was proved from sample SJ4 whose seismo radial grain velocity fractal dimension and capillary pressure fractal dimension was found to be 2.6843 as described in Table 1.

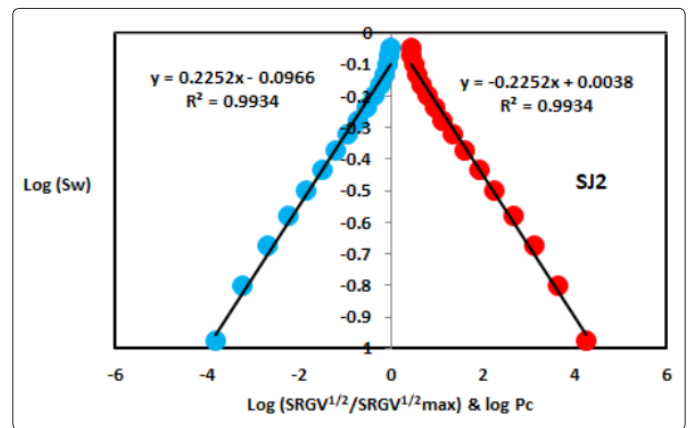


Figure 3: Log (SRGV^{1/2}/SRGV^{1/2}_{max}) & log pc versus log Sw for sample mple SJ2

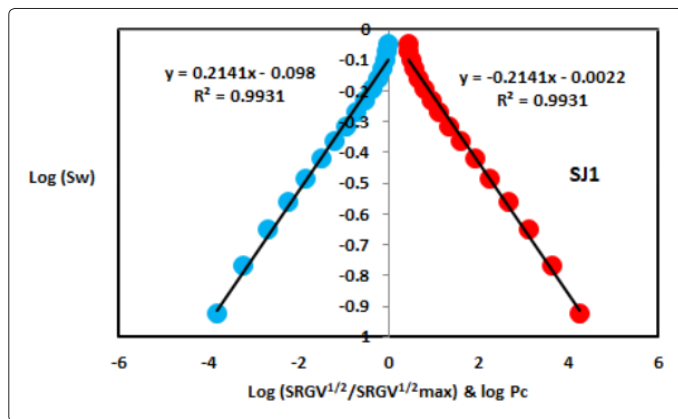


Figure 2: Log (SRGV^{1/2}/SRGV^{1/2}_{max}) & log pc versus log Sw for sample SJ1

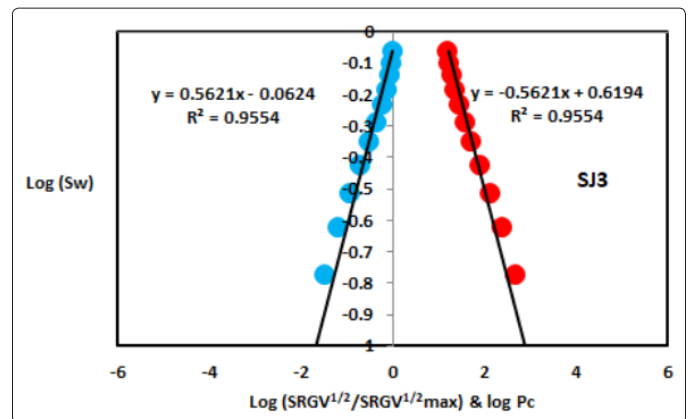


Figure 4: Log (SRGV^{1/2}/SRGV^{1/2}_{max}) & log pc versus log Sw for sample SJ3

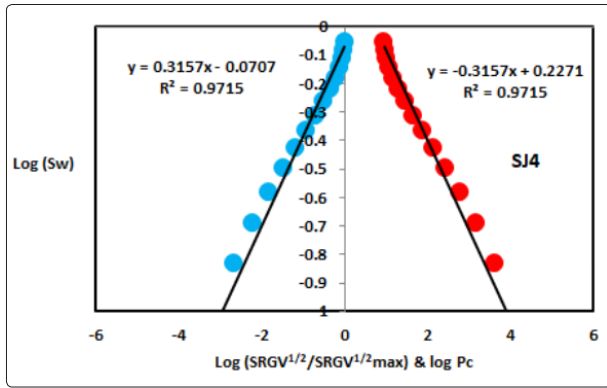


Figure 5: Log (SRGV^{1/2}/SRGV^{1/2}_{max}) & log pc versus log Sw for sample SJ4

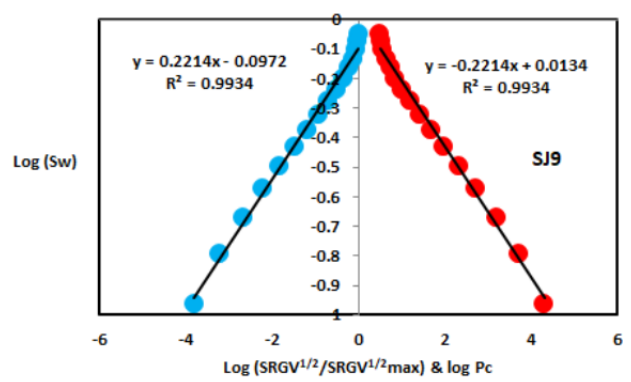


Figure 8: Log (SRGV^{1/2}/SRGV^{1/2}_{max}) & log pc versus log Sw for sample SJ9

In contrast, the Middle Shajara reservoir which is separated from the Lower Shajara reservoir by an unconformity surface as revealed in Figure 1. It was nominated by four samples (Figure 1), three of which named as SJ7, SJ8, and SJ9 as illuminated in Table 1 were chosen for capillary measurements as described in Table 1. Their positive slopes of the first procedure and negative slopes of the second procedure are shown in Figure 6, Figure 7 and Figure 8 and Table 1. Furthermore, their Seismo radial grain velocity fractal dimensions and capillary pressure fractal dimensions show similarities as defined in Table 1. Their fractal dimensions are higher than those of samples SJ3 and SJ4 from the Lower Shajara Reservoir due to an increase in their permeability as explained in table 1.

On the other hand, the Upper Shajara reservoir was separated from the Middle Shajara reservoir by yellow green mudstone as shown in Figure 1. It is defined by three samples so called SJ11, SJ12, SJ13 as explained in Table 1. Their positive slopes of the first procedure and negative slopes of the second procedure are displayed in Figure 9, Figure 10 and Figure 11 and Table 1. Moreover, their seismo radial grain velocity fractal dimension and capillary pressure fractal dimension are also higher than those of sample SJ3 and SJ4 from the Lower Shajara Reservoir due to an increase in their permeability as simplified in table 1.

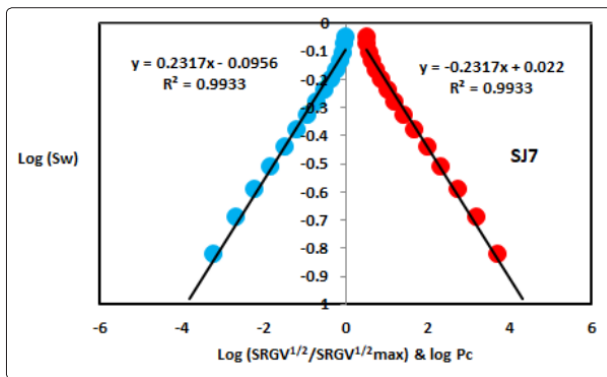


Figure 6: Log (SRGV^{1/2}/SRGV^{1/2}_{max}) & log pc versus log Sw for sample SJ7

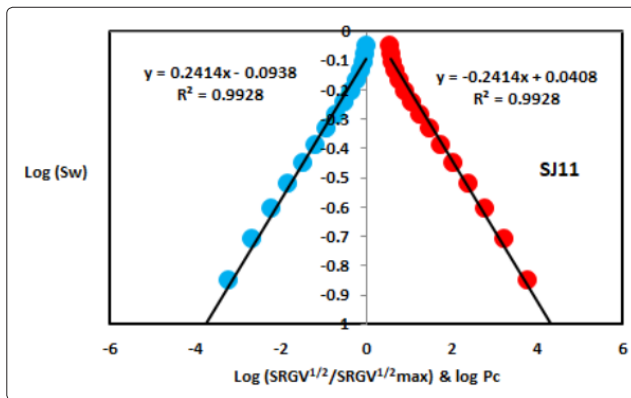


Figure 9: Log (SRGV^{1/2}/SRGV^{1/2}_{max}) & log pc versus log Sw for sample SJ11

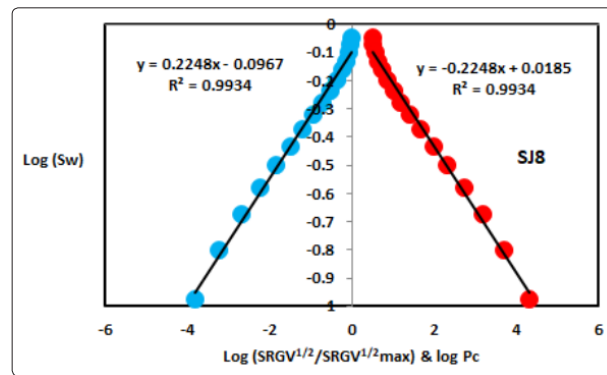


Figure 7: Log (SRGV^{1/2}/SRGV^{1/2}_{max}) & log pc versus log Sw for sample SJ8

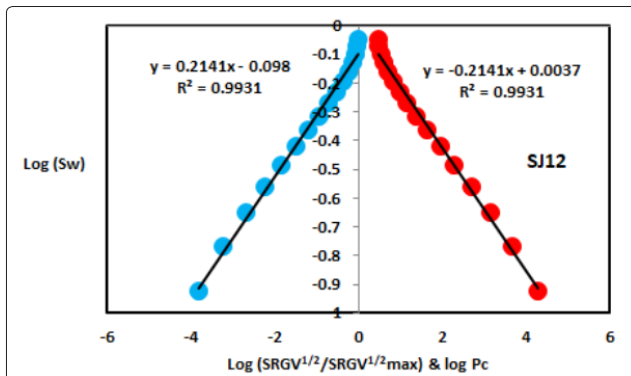


Figure 10: Log (SRGV^{1/2}/SRGV^{1/2}_{max}) & log pc versus log Sw for sample SJ12

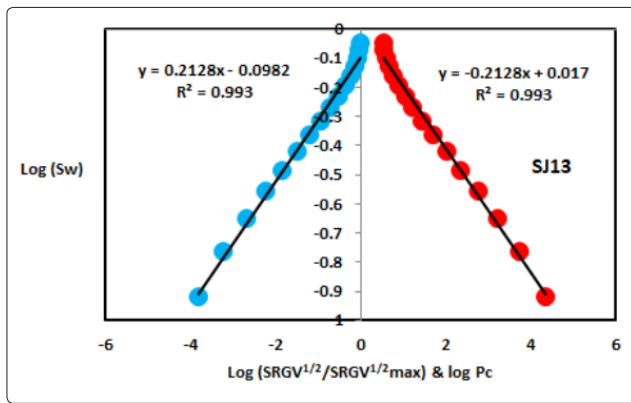


Figure 11: Log (SRGV^{1/2}/SRGV^{1/2}_{max}) & log pc versus log Sw for sample SJ13

Overall a plot of positive slope of the first procedure versus negative slope of the second procedure as described in Figure 12 reveals three permeable zones of varying Petrophysical properties. These reservoir zones were also confirmed by plotting seismo radial grain velocity fractal dimension versus capillary pressure fractal dimension as described in Figure 13. Such variation in fractal dimension can account for heterogeneity which is a key parameter in reservoir quality assessment.

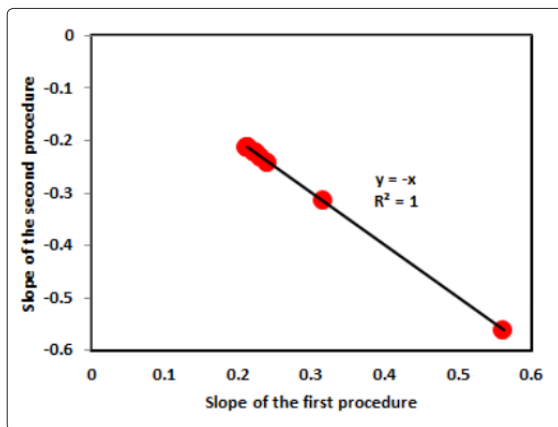


Figure 12: Slope of the first procedure versus slope of the second procedure

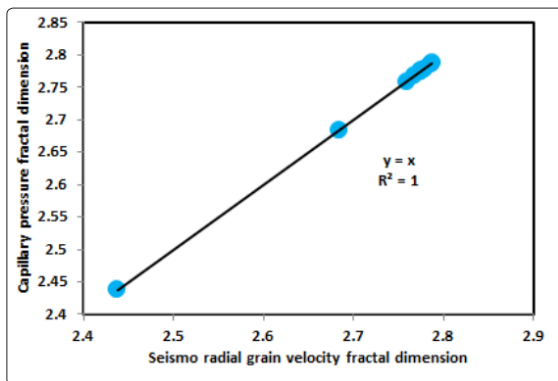


Figure 13: Seismo radial grain velocity fractal dimension versus capillary pressure fractal dimension

Conclusion

The sandstones of the Shajara Reservoirs of the permo-Carboniferous Shajara Formation were divided here into three units based on seismo radial grain velocity fractal dimension. The Units from base to top are: Lower Shajara Seismo Radial Grain Velocity Fractal Dimension Unit, Middle Shajara Seismo Radial Grain Velocity Fractal Dimension Unit, and Upper Shajara Seismo Radial Grain Velocity Fractal Dimension Unit. These units were also proved by capillary pressure fractal dimension. The fractal dimension was found to increase with increasing grain size and permeability owing to possibility of having interconnected channels.

Acknowledgement

The author would to thank King Saud University, college of Engineering, Department of Petroleum and Natural Gas Engineering, Department of Chemical Engineering, Research Centre at College of Engineering, College of science, Department of Geology, and King Abdullah Institute for research and Consulting Studies for their supports.

References

1. Frenkel J (1944) On the theory of seismic and seismoelectric phenomena in a moist soil. *Journal of physics* 3: 230-241.
2. Li K, Williams W (2007) Determination of capillary pressure function from resistivity data. *Transport in Porous Media* 67: 1-15.
3. Revil A, Jardani A (2010) Seismo electric response of heavy oil reservoirs: theory and numerical modelling. *Geophysical J International* 180: 781-797.
4. Dukhin A, Goetz P, Thommes M (2010) Seismoelectric effect: a non-isochoric streaming current.1 Experiment. *J Colloid Interface Sci* 345: 547-553.
5. Guan W, Hu H, Wang Z (2012) Permeability inversion from low-frequency seismoelectric logs in fluid- saturated porous formations. *Geophys Prospect* 61: 120-133.
6. Hu H, Guan W, Zhao W (2012) Theoretical studies of permeability inversion from seismoelectric logs. *Geophysical Research Abstracts* 14: EGU2012-6725-1 2012 EGU General Assembly.
7. Borde C, Sen echal P Barri`ere J, Brito D, Normandin E et al., (2015) Impact of water saturation on seismoelectric transfer functions: a laboratory study of co-seismic phenomenon. *Geophysical J International* 200: 1317-1335.
8. Jardani A, Revil A (2015) Seismoelectric couplings in a poroelastic material containing two immiscible fluid phases. *Geophysical Journal International* 202: 850-870.
9. Holzhauser J, Brito D, Bordes C, Brun Y, Guatarbes B (2016) Experimental quantification of the seismoelectric transfer function and its dependence on conductivity and saturation in loose sand. *Geophys Prospect* 65: 1097-1120
10. Rong Peng, Jian-Xing Wei, Bang-Rang Di, Pin-Bo Ding, ZiChun Liu (2016) Experimental research on seismoelectric effects in sandstone. *Applied Geophysics* 13: 425-436.
11. Djuraev U, Jufar S R, Vasant P (2017) Numerical Study of frequency-dependent seismo electric coupling in partially saturated porous media. *MATEC Web of Conferences* 87, 02001.
12. Alkhidir KEME (2020) Seismo Magnetic Moment Fractal Dimension for Characterizing Shajara Reservoirs of the PermoCarboniferous Shajara Formation, Saudi Arabia *World Scientific News* 139: 186-200.

-
13. Alkhidir KEME (2019) Seismo Diffusion Coefficient Fractal Dimension for Characterizing Shajara Reservoirs of the Permo-Carboniferous Shajara Formation, Saudi Arabia. Research Journal of Nanoscience and Engineering 3 : 23-29.
 14. Alkhidir KEME (2019). Molar Enthalpy Fractal Dimension for Characterizing Shajara Reservoirs of the Permo-Carboniferous Shajara Formation. Journal of Agriculture and Aquaculture 1: 1-8.
 15. Alkhidir KEME (2019) Work Fractal Dimension for Characterizing Shajara Reservoirs of the PermoCarboniferous Shajara Formation, Saudi Arabia. Int J Environ & Agri Sci 3: 1-8
 16. Alkhidir KEME (2018) Electro Kinetic Fractal Dimension for Characterizing Shajara Reservoirs of the Shajara Formation. Int J Nano Med & Eng. 3: 54-60.
 17. Al-Khidir KE (2018) On Similarity of Pressure Head and Bubble Pressure Fractal Dimensions for Characterizing Permo-Carboniferous Shajara Formation, Saudi Arabia. J Indust Pollut Toxic 1: 102.

Copyright: ©2020 Khalid Elyas Mohamed Elameen Alkhidir. This is an open-access article distributed under the terms of the Creative Commons Attribution License, which permits unrestricted use, distribution, and reproduction in any medium, provided the original author and source are credited.